Effects of Temperature and Composition on Catholyte Stability in Vanadium Flow Batteries: Measurement and Modeling

Daniela Oboroceanu,[a] Nathan Quill,[a] Catherine Lenihan,[a] Deirdre Ní Eidhin,[a] Sergiu P. Albu,[a] Robert P. Lynch,[a,*,z] and D. Noel Buckley[a,b,]**

[a]*Department of Physics, Bernal Institute, University of Limerick, Limerick, Ireland*
[b]*Department of Chemical and Biomolecular Engineering, Case Western Reserve University, Cleveland, Ohio, USA*

The stability of typical vanadium flow battery (VFB) catholytes was investigated at temperatures in the range 30–60°C for V^V concentrations of 1.4–2.2 mol dm^{-3} and sulfate concentrations of 3.6–5.4 mol dm^{-3}. In all cases, V_2O_5 precipitates after an induction time, which decreases with increasing temperature. Plots of the logarithm of induction time versus the inverse of temperature (equivalent to Arrhenius plots) show excellent linearity and all have similar slopes. The logarithm of induction time also increases linearly with sulfate concentration and decreases linearly with V^V concentration. The slopes of these plots give values of concentration coefficients β_S and β_{V5} which were used to normalize induction times to reference concentrations of sulfate and V^V. An Arrhenius plot of the normalized induction times gives a good straight line, the slope of which yields a value of 1.791 ± 0.020 eV for the activation energy. Combining the Arrhenius equation with the observed variation with sulfate and V^V concentrations, an equation was derived for the induction time for any catholyte at any temperature in the range investigated. Although the mechanism of precipitation of V^V from catholytes is not yet well understood, a precise activation energy can now be assigned to the induction process.

Manuscript received May 11, 2017. Published July 19, 2017. This was Paper 32 presented at the Honolulu, Hawaii, Meeting of the Society, October 2–7, 2016.

The rapid growth of renewable electricity generation from intermittent sources such as solar photovoltaic and wind is driving a need for advanced, cost-effective, electrical energy storage (EES) technologies.[1–3] Redox flow batteries[4–11] (RFBs) have attracted much interest for large-scale energy storage due to advantages over other EES technologies, and research activities in this area have grown exponentially in recent years.[12,13] The energy storage capability and power output of a flow battery, unlike conventional batteries, can be scaled independently to suit the desired application.[7] Other advantages[14] include a high degree of safety, long lifetime, potentially low capital costs, high reliability and relatively high energy efficiency.

Among the numerous systems that have been studied, the vanadium flow battery (VFB), also known as the vanadium redox flow battery (VRFB), is commonly regarded as one of the most promising.[5–7,15–17] The chemistry of this system is perhaps the most thoroughly characterized and the cell design has been considerably optimized.[2,18,19] It has seen the widest commercial deployment[17] and systems as large as 250–1000 kWh have been demonstrated.[20] Compared to other flow battery systems, VFBs have the additional advantage that cross-contamination due to transport through the separating membrane is effectively eliminated because the anolyte and catholyte differ only in the oxidation state of the vanadium.[21] As a result, electrolyte maintenance issues are reduced; in theory, the electrolyte is indefinitely reuseable. Furthermore, if rebalancing of the system is required the electrolytes in the two reservoirs can be mixed with each other. Since aqueous vanadium species are highly colored, the vanadium concentrations and state-of-charge of both sides of a VFB may be precisely monitored using ultraviolet-visible (UV-vis) spectroscopy.[22,23] Active areas of research on VFBs include cell design and modeling,[7,24,25] performance and state-of-charge (SoC) monitoring,[22,23,26–30] coulombic and energy efficiencies,[31,32] electrolytes,[29,30,33,34] membranes,[35] and electrodes.[10,36–68]

The solubility of each of the vanadium species, V^{II}, V^{III}, V^{IV} and V^V, is an important factor affecting the energy density of VFBs. The V^{II}, V^{III} and V^{IV} species (i.e., V^{2+}, V^{3+} and VO^{2+}) are generally quite soluble in strongly acidic H_2SO_4 or H_2SO_4-HCl solutions; generally their solubility increases with temperature and decreases with increasing acid concentration.[69] The predominant V^V species[70] present in strongly acidic solutions is the pervanadyl ion VO_2^+. The solubility of vanadium (V) oxide, V_2O_5, at the pH of typical VFB catholytes is ∼0.1 mol dm^{-3} or less[71] and so VO_2^+ is expected to be thermodynamically unstable in solution with respect to precipitation as V_2O_5. Nevertheless, catholytes with high concentrations of V^V (> 1.5 mol dm^{-3}) in sulfuric acid can persist for very long periods of time. The stability of these metastable solutions (VFB catholytes) decreases, as expected, as the concentration of V^V increases.[72] This is reflected in a lowering of stability at a particular vanadium concentration as the SoC (i.e. the fraction of vanadium present as V^V) of the catholyte increases.[33] Stability improves with increasing concentration of sulfate[73] and in the presence of certain additives[6,74] such as H_3PO_4.

Although several studies[33,72–78] have been reported on the stability of V^V in the catholyte of VFBs and several mechanisms of precipitation have been proposed,[75,76] there is a lack of detailed kinetic studies of the process leading to precipitation and of quantitative analysis of the variation with temperature. Recently, we communicated a preliminary report[79] which shows that precipitation of V^V from sulfuric acid solution occurs after an induction time that increases exponentially with the inverse of temperature, i.e. shows Arrhenius behavior.[80] In this paper we report more detailed investigation and analysis of this behavior and present a comprehensive model for the stability of V^V in acidic sulfate electrolytes.

Arrhenius Analysis

When a typical VFB catholyte is held at constant temperature it eventually precipitates V_2O_5 after an induction time τ which depends on the temperature. The kinetics of the processes occurring in solution during the induction period are not easy to characterize, and the nature of these processes is not yet well understood. However the induction time τ may be measured[79] with good precision simply by observing the time at which the first precipitate forms and, as indicated above, we have shown that the logarithm of the induction time increases linearly with the inverse of temperature. Thus, using the Arrhenius equation we can analyze the effect of temperature on the kinetics based on the

*Electrochemical Society Member.
**Electrochemical Society Fellow.
[z]E-mail: Robert.Lynch@UL.ie

measured induction times. In this section, we discuss the theoretical underpinnings of such an analysis.

Fig. 1a schematically represents the progress of the process occurring in the catholyte during the induction period in terms of an extent of reaction α. For a general kinetic rate law

$$\frac{\delta\alpha}{\delta t} = k(T) f(\alpha) \quad [1]$$

where t is time, T is temperature, $f(\alpha)$ is some function of α, and $k(T)$ is the temperature-dependent rate constant, the Arrhenius equation may be written as

$$k(T) = A \exp\left[-\frac{E^{\#}}{k_B T}\right] \quad [2]$$

where A is a constant called the pre-exponential term, $E^{\#}$ is the apparent activation energy and k_B is Boltzmann's constant.[80–85] Thus

$$\frac{\delta\alpha}{\delta t} = A\left[\exp\left\{-\frac{E^{\#}}{k_B T}\right\}\right] f(\alpha). \quad [3]$$

For any given value of α and two temperatures T and T_0

$$\frac{\left[\frac{\delta\alpha}{\delta t}\right]_T}{\left[\frac{\delta\alpha}{\delta t}\right]_{T_0}} = \frac{\exp\left\{-\frac{E^{\#}}{k_B T}\right\}}{\exp\left\{-\frac{E^{\#}}{k_B T_0}\right\}} \quad [4]$$

and so

$$\left[\frac{\delta\alpha}{\delta t}\right]_T = \left[\frac{\delta\alpha}{\delta t}\right]_{T_0} \exp\left\{\frac{E^{\#}}{k_B}\left(\frac{1}{T_0} - \frac{1}{T}\right)\right\}. \quad [5]$$

Since the extent of reaction α is a strictly increasing function of time t, we can consider t to be a well-defined function of α. This is represented in Fig. 1b, which shows a schematic plot of t versus α corresponding to the plot of α versus t in Fig. 1a. The derivative ($\delta t/\delta\alpha$) of the curve in Fig. 1b is

$$\left[\frac{\delta t}{\delta\alpha}\right]_T = \left(\left[\frac{\delta\alpha}{\delta t}\right]_T\right)^{-1} = \left[\frac{\delta t}{\delta\alpha}\right]_{T_0} \exp\left\{\frac{E^{\#}}{k_B}\left(\frac{1}{T} - \frac{1}{T_0}\right)\right\} \quad [6]$$

A schematic plot of ($\delta t/\delta\alpha$) is shown in Fig. 1c.

We now consider a system in an initial state represented by an extent of reaction $\alpha = \alpha_1$ at $t = t_1$. At a temperature T_0, the time interval τ_0 for this system to reach (at $t = t_2$) an extent of reaction $\alpha = \alpha_2$ may be expressed as

$$\tau_0 = t_2 - t_1 = \int_{\alpha_1}^{\alpha_2} \left[\frac{\delta t}{\delta\alpha}\right]_{T_0} d\alpha \quad [7]$$

(see Fig. 1c). Similarly if the system were at a temperature T, the time to progress from $\alpha = \alpha_1$ to $\alpha = \alpha_2$ would be

$$\tau = \int_{\alpha_1}^{\alpha_2} \left[\frac{\delta t}{\delta\alpha}\right]_T d\alpha$$

$$= \int_{\alpha_1}^{\alpha_2} \left[\exp\left\{\frac{E^{\#}}{k_B}\left(\frac{1}{T} - \frac{1}{T_0}\right)\right\}\right]\left[\frac{\delta t}{\delta\alpha}\right]_{T_0} d\alpha \quad [8]$$

from Equation 6. Since T and T_0 are constant for the integration, Equation 8 becomes

$$\tau = \left[\exp\left\{\frac{E^{\#}}{k_B}\left(\frac{1}{T} - \frac{1}{T_0}\right)\right\}\right] \int_{\alpha_1}^{\alpha_2} \left[\frac{\delta t}{\delta\alpha}\right]_{T_0} d\alpha \quad [9]$$

$$= \left[\exp\left\{\frac{E^{\#}}{k_B}\left(\frac{1}{T} - \frac{1}{T_0}\right)\right\}\right] \tau_0 \quad [10]$$

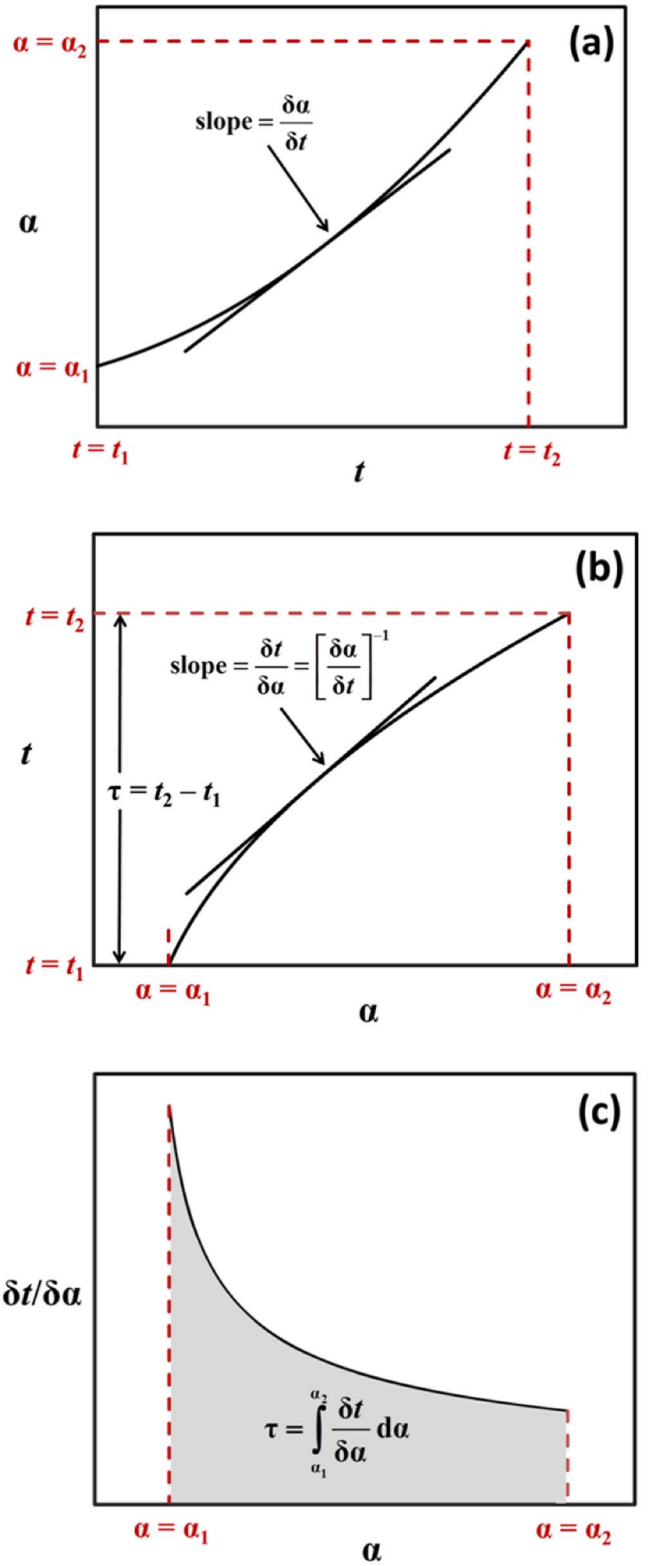

Figure 1. (a) Schematic plot of extent of reaction α versus time t at constant temperature for the process occurring in the catholyte during the induction period for precipitation; (b) corresponding plot of t versus α; and (c) the derivative ($\delta t/\delta\alpha$) of the curve in (b) plotted versus α.

from Equation 7. Thus

$$\tau = D\tau_0 \quad [11]$$

where

$$D = \exp\left\{\frac{E^{\#}}{k_B}\left(\frac{1}{T} - \frac{1}{T_0}\right)\right\} = \frac{k(T_0)}{k(T)}$$

from Equation 2.

The value of D depends only on T and T_0 and so Equation 11 represents a principle that we call the proportionality of corresponding times:[83] for given temperatures T and T_0 the corresponding times τ and τ_0 are related by the same proportionality factor D for all choices of (α_1,α_2). We note that if the average rate of the process during the induction period τ at temperature T is

$$r = \left(\frac{\delta\alpha}{\delta t}\right)_{\text{avg},T} = \frac{\alpha_2 - \alpha_1}{\tau}$$

and r_0 is the value of r at temperature T_0, then

$$\frac{r}{r_0} = \frac{\alpha_2 - \alpha_1}{\tau}.\frac{\tau_0}{\alpha_2 - \alpha_1} = \frac{\tau_0}{\tau} = \frac{1}{D}.$$

The fact that D is independent of choice of the initial and final states, α_1 and α_2, enables a straightforward Arrhenius analysis of a rate process where observations are possible only for a limited number of states.[83–85] From Equation 10,

$$\ln\tau = \frac{E^{\#}}{k_B}\left(\frac{1}{T} - \frac{1}{T_0}\right) + \ln\tau_0 = B + \frac{E^{\#}}{k_B T} \quad [12]$$

where

$$B = \ln\tau_0 - \frac{E^{\#}}{k_B T_0} \quad [13]$$

Thus, in the present case, we can measure the time interval τ between the initial state α_1 when the sample is set to the test temperature and the final state α_2 at which precipitation is observed to occur. We assume that the system passes through intermediate states but we cannot directly observe these states in our investigation. In fact we cannot determine any specific rate law for the reaction and we can only speculate on the actual processes or reactions that are occurring during the induction period. Nevertheless, we can measure the induction time τ at a series of temperatures T. According to Equation 12, a plot of $\ln\tau$ versus $1/T$ should give a straight line if the apparent activation energy $E^{\#}$ is constant over the temperature range. From the slope $m = \frac{E^{\#}}{k_B}$ of this plot we can determine a value of $E^{\#}$; the intercept on the $\ln\tau$ axis is B.

Experimental

Solutions of V^{IV} were prepared from $VOSO_4$ and H_2SO_4 (vanadyl (IV) sulfate hydrate 97% and sulfuric acid 98% obtained from Sigma Aldrich). Stock solutions of V^V were prepared by electrochemical oxidation of the V^{IV} solution in a flow cell at room temperature (~20°C) using carbon felt electrodes and a Nafion membrane. End-points were determined by monitoring the potential (using 1.3 V vs Ag/AgCl at 10 mA cm^{-3} as end point) and verified by color changes in the electrolyte. These solutions were stored at ~4°C and used to prepare series of other concentrations of V^V by dilution with known concentrations of H_2SO_4. Because samples were relatively small (~10 cm^3), volumes were measured by weighing and converting to volume by accurately measured densities. Vanadium concentrations were determined against standard 0.1 N $KMnO_4$ (Fisher Scientific) and H_2SO_4 concentrations were determined against standard 0.1 N KOH (Sigma-Aldrich). Water was distilled and deionized to a resistivity of >18 MΩ cm.

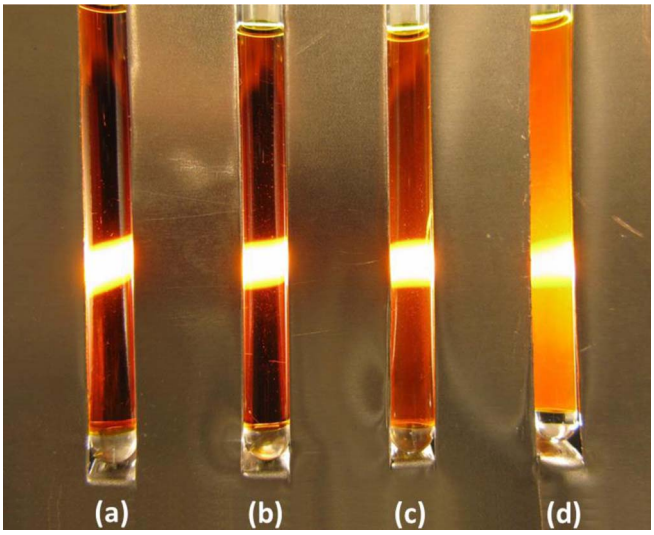

Figure 2. Photograph showing vials of catholyte solution after immersion in a water bath at 60°C for (a) 0 s (i.e. not immersed), (b) 1500 s, (c) 1740 s, and (d) 2190 s. The solution had a V^V concentration of 1.84 mol dm^{-3} and a total sulfate concentration of 4.2 mol dm^{-3}. The vials are back-illuminated by a long, horizontal fluorescent tube behind a slotted metal screen – the image of the tube is visible on the vials.

In a typical experiment, 0.8 cm^3 samples of solutions with selected concentrations of V^V and sulfate[c] were placed in small glass vials (7 cm in length × 4.6 mm internal diameter). The vials were then immersed in a thermostatic water bath which had been equilibrated at a selected temperature and the time of immersion was recorded: the solution temperature reached a value within 0.1 K of the bath temperature in ~60 s. The time at which precipitation was observed in each of the separate vials was subsequently recorded. The water-bath reservoir was made of transparent glass and was illuminated from underneath by a lamp so that the solution in the vial was very clearly visible and the first signs of precipitation could be observed.[79,86] Since the measured induction times ranged from 2.7×10^3 s to 5.9×10^5 s, the worst-case uncertainty due to temperature ramp-up was less than ~2%, and much less in most cases.

Results and Discussion

Variation of induction time with temperature.—Fig. 2 shows a sequence of images of vials of V^V solution incubated in the water bath for different times at 60°C. Fig. 2a shows a vial before immersion in the water bath. Fig. 2b, obtained after the vial had been in the water bath for 1500 s, shows no visible change in the solution. Fig. 2c, after 1740 s, shows some change from (a) and (b) in that there is a small amount of scattered light (slightly cloudy appearance). However Fig. 2d, after 2190 s, shows a very obvious change with a lot of scattered light giving a cloudy appearance. Careful observation of the vial in Fig. 2d shows signs of precipitation and, in fact, a precipitate settles to the bottom when the solution is allowed to stand for some hours. This does not happen with the other vials (Figs. 2a–2c). These images were obtained by removing the vials from the water bath and back-lighting them using a long, horizontal fluorescent tube behind a slotted metal screen. However, the change observed in Fig. 2d, corresponding to the onset of precipitation, can also be observed by direct visual observation in the transparent water bath (as described in

[c]The term *sulfate concentration* in this paper is used to include HSO_4^- (which predominates), SO_4^{2-}, and H_2SO_4, and is represented as [S], i.e. total sulfur.

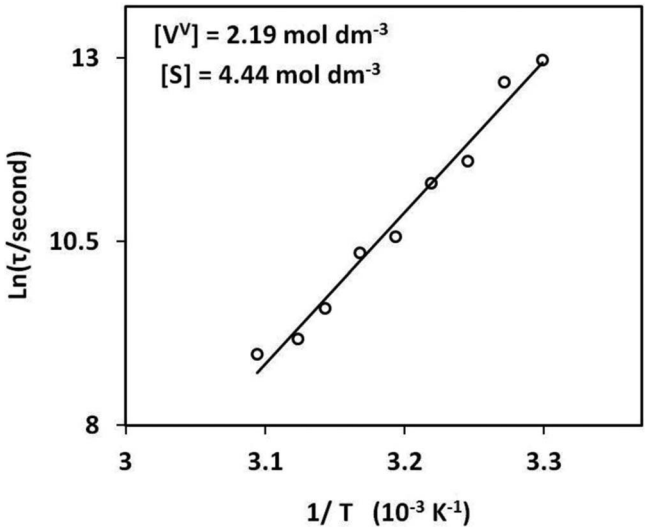

Figure 3. Arrhenius plot of induction time for a vanadium concentration of 2.19 mol dm^{-3} and a sulfate concentration of 4.44 mol dm^{-3}.

the Experimental section) and the time at which precipitation occurs can be precisely determined in this way.

Series of experiments were carried out in which the induction time for precipitation was measured as described above for a range of temperatures. Typical results are shown in Fig. 3 where the logarithm of induction time for a typical catholyte sample is plotted against the inverse of temperature. As discussed above, this is equivalent to an Arrhenius plot. It can be seen that good linearity is obtained over the temperature range investigated (30–60°C), indicating that the process occurring during the induction period is kinetically controlled and that its activation energy is constant over this temperature range. From the slope, $m = 2.072 \times 10^4$ K, of the graph the activation energy ($E^{\#} = mk_B$ where k_B is Boltzmann's constant) is estimated to be 1.79 eV (172 kJ mol^{-1}).

Similar experiments were carried out for other catholyte compositions (various concentrations of V^V and sulfate). The resulting Arrhenius plots (similar to that in Fig. 3) are shown in Fig. 4 for a range of concentrations of V^V at each of three different concentrations of sulfate. The slopes and intercepts of the least-squares best-fit lines of the Arrhenius plots for the various catholyte compositions are shown in Table I. All of the lines have similar slopes: the average slope of the lines with six or more data points is $(2.116 \pm 0.061) \times 10^4$ K representing a standard deviation of less than 3%. This indicates that the activation energy does not change significantly for the range of compositions investigated (~1.4 mol dm^{-3} < [V^V] < ~2.2 mol dm^{-3} and ~3.7 mol dm^{-3} < [S] < ~5.4 mol dm^{-3}). It is also clear from Fig. 4 that the induction time decreases with increasing concentration of V^V at any given concentration of sulfate.

Arrhenius plots at a vanadium concentration of 1.66 mol dm^{-3} for each of three sulfate concentrations are compared in Fig. 5; it is clear that induction time increases with increasing concentration of sulfate. A similar trend can be observed at other concentrations of V^V (see Fig. 4).

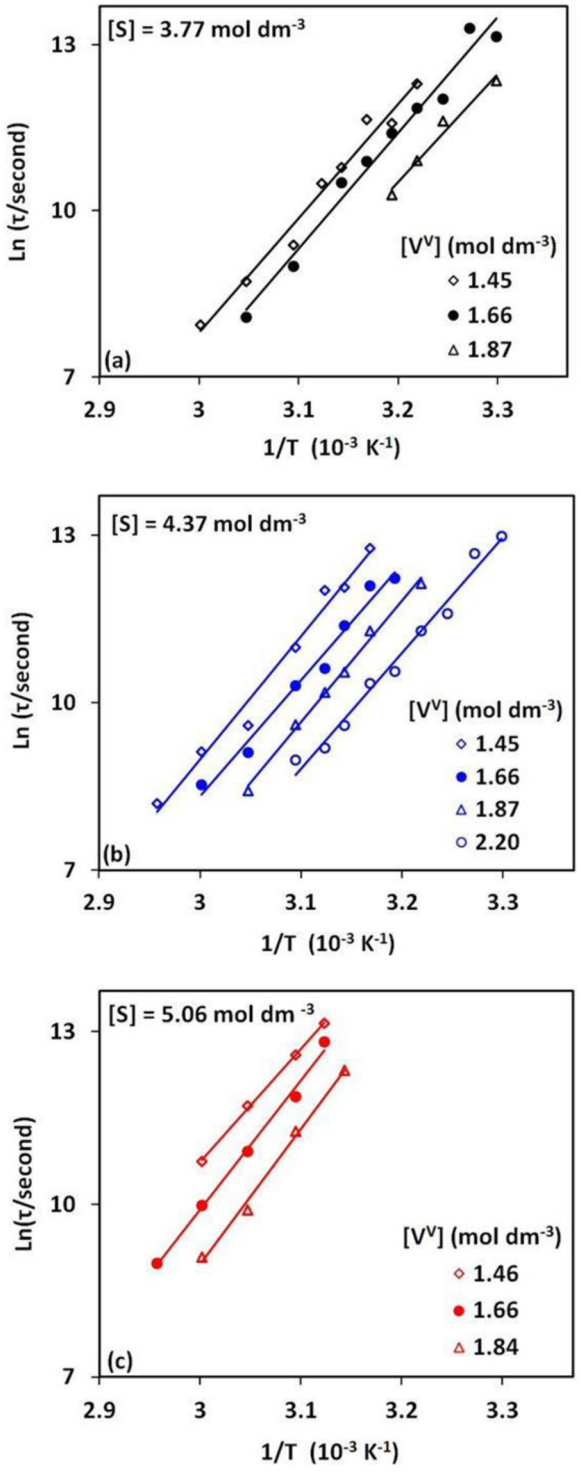

Figure 4. Arrhenius plots of induction time for various concentrations of V^V at a sulfate concentration of (a) 3.77, (b) 4.37, and (c) 5.06 mol dm^{-3}.

Effect of concentrations of sulfate and V^V.—The effect of sulfate concentration was investigated in more detail in an additional series of experiments at a constant V^V concentration of 1.76 mol dm^{-3}. The results of these experiments are shown in Table II. To quantitatively compare the induction times at the different sulfate concentrations, a comparison temperature of 50°C (T_c = 323.15 K) was selected. The measured induction time τ_T at each temperature was converted to the logarithm of the induction time ln τ_{T_c} at the comparison temperature by the equation

$$\ln\ \tau_{T_c} = \ln\ \tau_T + m\left(\frac{1}{T_c} - \frac{1}{T}\right) \qquad [14]$$

using the average value of Arrhenius slope $m = 2.116 \times 10^4$ K from Table I. The resulting values of ln τ_{T_c} are shown in Table II and are plotted against sulfate concentration in Fig. 6. A good fit to a straight line is obtained. This indicates that the logarithm of the induction time increases linearly with the sulfate concentration, i.e., the induction

Table I. Slopes and intercepts of Arrhenius plots of induction time for catholyte solutions with various concentrations of vanadium and sulfate.

Solution Code	Concentration of V^V (mol dm^{-3})	Concentration of sulfate (mol dm^{-3})	Slope, m (K)	Intercept, B_R	Coefficient of Determination, R^2	Number of Data Points
D13	1.45	5.37	17318	−40.486	0.9826	3
D14	1.66	5.40	19453	−47.630	0.9898	3
D17	1.46	5.07	19592	−48.038	0.9990	4
D18	1.66	5.09	22366	−57.190	0.9942	5
D19	1.84	5.03	23565	−61.741	0.9922	4
D22	1.45	4.35	22113	−57.354	0.9820	7
D23	1.66	4.37	20736	−53.889	0.9800	7
D24	1.87	4.37	21743	−57.751	0.9940	6
D25	2.02	4.38	22133	−59.518	0.9974	4
P01	2.20	4.40	20723	−55.417	0.9825	9
D28	1.45	3.77	20694	−54.290	0.9780	8
D29	1.66	3.78	20942	−55.604	0.9776	9
D30	1.87	3.77	19455	−51.727	0.9711	4

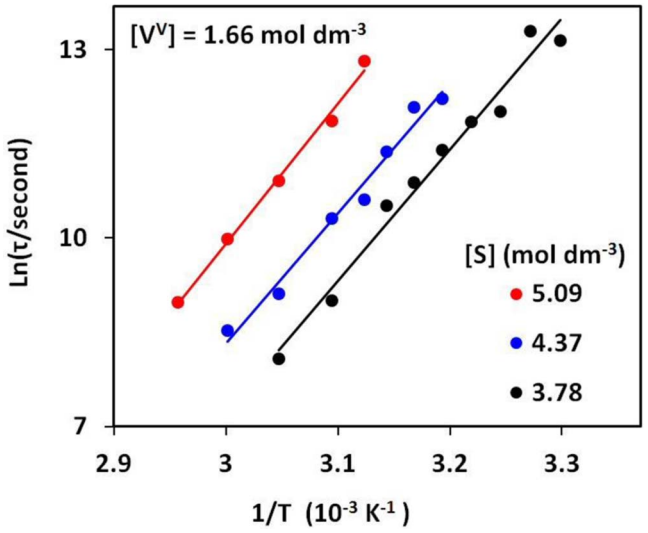

Figure 5. Arrhenius plots of induction time for various concentrations of sulfate at a V^V concentration of 1.66 mol dm^{-3}.

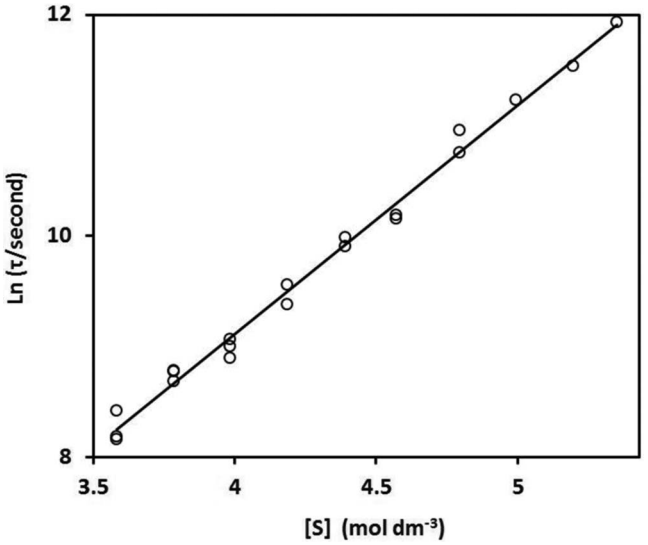

Figure 6. Natural logarithm of induction time at 50°C for a vanadium concentration of 1.76 mol dm^{-3} plotted against sulfate concentration.

time increases exponentially with the sulfate concentration. The slope of this line is the fractional rate of variation of induction time with sulfate concentration

$$\beta_S = \frac{\partial \ln \tau}{\partial [S]} = \frac{1}{\tau}\frac{\partial \tau}{\partial [S]} \quad [15]$$

where τ is the induction time and [S] is the total concentration of sulfate. The slope of the least-squares best-fit line in Fig. 6 gives a value of $\beta_S = 2.073$ mol^{-1} dm^3. Since the Arrhenius slope does not vary significantly with concentration of V^V, this value of β_S holds for all temperatures in the range investigated. We call β_S the sulfate concentration coefficient of induction time.

We can use β_S to estimate values of ln τ standardized to a selected sulfate concentration $[S]_R$ from the values measured at a concentration $[S]_M$ at the same temperature. Thus, at any given V^V concentration the standardized value of ln τ is

$$\ln \tau_R = \ln \tau_M + \beta_S([S]_R - [S]_M) \quad [16]$$

Table II. Measured induction time τ_T for catholyte solutions with various sulfate concentrations at several temperatures. The logarithms of τ_T and of the estimated induction times τ_{T_c} at a comparison temperature of 50°C are also shown. The total V^V concentration was 1.76 mol dm^{-3} in each case.

Solution Code	[S] (mol dm^{-3})	Temperature (°C)	Time, τ_T (10^4 s)	ln τ_T	ln τ_{T_c}
D01	3.58	45.0	1.002	9.212	8.183
	3.58	40.0	3.666	10.509	8.419
	3.58	35.0	8.478	11.348	8.161
D02	3.79	45.0	1.662	9.718	8.689
	3.79	40.0	5.214	10.862	8.771
	3.79	35.0	15.732	11.966	8.779
D03	3.98	45.0	2.262	10.027	8.998
	3.98	40.0	7.002	11.157	9.066
	3.98	35.0	17.73	12.086	8.898
D04	4.19	45.0	3.306	10.406	9.377
	4.19	40.0	11.46	11.649	9.558
D05	4.39	45.0	5.622	10.937	9.908
	4.39	40.0	17.634	12.080	9.989
D06	4.57	60.0	0.372	8.221	10.187
	4.57	45.0	7.224	11.188	10.159
D07	4.79	60.0	0.804	8.992	10.958
	4.79	45.0	13.038	11.778	10.749
D08	4.99	60.0	1.053	9.262	11.227
D09	5.20	60.0	1.428	9.567	11.532
D10	5.35	60.0	2.136	9.969	11.935

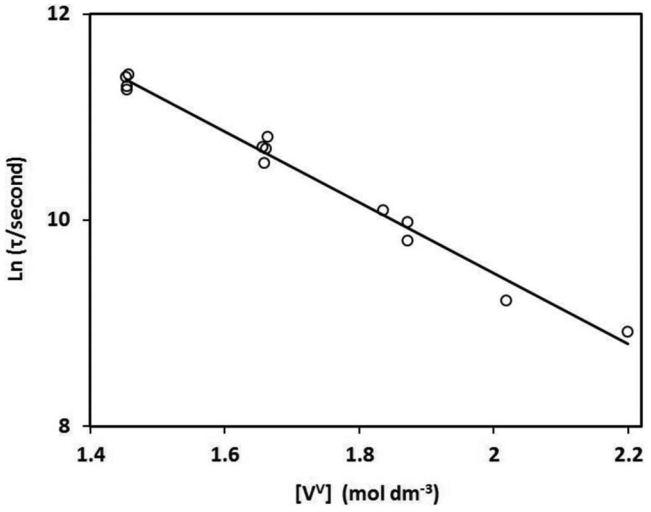

Figure 7. Natural logarithm of induction time at 50°C for a sulfate concentration of 4.5 mol dm^{-3} plotted against vanadium concentration.

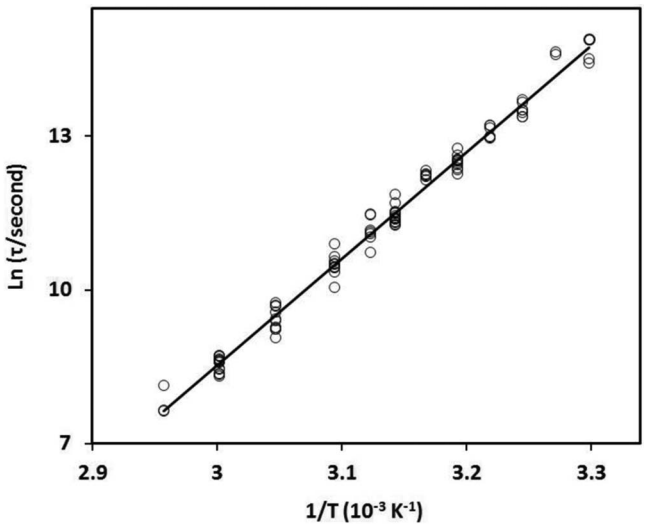

Figure 8. Arrhenius plot of induction time for the solutions shown in Tables I and II. The measured induction times have been normalized to concentrations $[S]_R = 4.5$ mol dm^{-3} and $[V^V]_R = 1.7$ mol dm^{-3}.

where of τ_M is the value of τ measured at a sulfate concentration $[S]_M$. But ln τ_M can be expressed by the Arrhenius Equation

$$\ln\ \tau_M = B + \frac{m}{T} \qquad [17]$$

and so

$$\ln\ \tau_R = B + \frac{m}{T} + \beta_S([S]_R - [S]_M) \qquad [18]$$

where m and B are the Arrhenius slope and intercept, respectively, measured for an electrolyte with sulfate concentration $[S]_M$.

Using Equation 18 we estimated standardized values of ln τ_R for each of the solutions in Table I from its measured Arrhenius parameters B_R and m with $\beta_S = 2.073$ mol^{-1} dm^3. These values, referenced to a sulfate concentration $[S]_R = 4.5$ mol dm^{-3} and a temperature of 50°C, are plotted against V^V concentration in Fig. 7. A good fit to a straight line is obtained, indicating that the logarithm of the induction time decreases linearly as the V^V concentration increases. The slope of this line is the fractional rate of variation of induction time with V^V concentration

$$\beta_{V5} = \frac{\partial \ln \tau}{\partial [V^V]} = \frac{1}{\tau}\frac{\partial \tau}{\partial [V^V]} \qquad [19]$$

where $[V^V]$ is the concentration of V^V. The slope of the least-squares best-fit line in Fig. 7 gives a value of $\beta_{V5} = -3.434$ mol^{-1} dm^3. We call β_{V5} the V^V concentration coefficient of induction time. The value of β_{V5} must be approximately constant over the ranges of concentration of V^V (1.4–2.2 mol dm^{-3}) and sulfate (3.6–5.4 mol dm^{-3}) since Fig. 7 contains data over these ranges. The good linear fit in Fig. 7 also indicates that the value of β_S (estimated as 2.073 mol^{-1} dm^3 at a V^V concentration of 1.76 mol dm^{-3}) must be approximately constant for all V^V and sulfate concentrations in the range investigated, since the same value of β_S was used to adjust all of the measured values of τ to the plotted values.

Analysis and modeling of induction time.—We can use the coefficients β_S and β_{V5} to convert the measured induction time τ at concentrations [S] and $[V^V]$ to a standard value τ_R with respect to reference concentrations $[S]_R$ and $[V^V]_R$ at the same temperature, T. Thus

$$\ln\ \tau_R = \ln\ \tau + \beta_S([S]_R - [S]) + \beta_{V5}([V^V]_R - [V^V]) \qquad [20]$$

Using Equation 20, all measured values of ln τ (summarized in Tables I and II) were standardized to reference concentrations $[S]_R = 4.5$ mol dm^{-3} and $[V^V]_R = 1.7$ mol dm^{-3}. An Arrhenius plot of the resulting values is shown in Fig. 8. The plot shows good linearity; the slope and intercept of the least-squares best-fit line are $m = 20785$ K and $B_R = -53.828$ respectively.

Thus 93 separate experimental values of ln τ measured for 23 different electrolyte solutions with V^V concentrations of 1.4–2.2 mol dm^{-3} and sulfate concentrations of 3.6–5.4 mol dm^{-3} over a temperature range of 30–65°C all fall on a good linear Arrhenius plot. The standard error of estimate of the slope is 238 K (1.1%); the activation energy estimated from the slope is $E^{\#} = (1.791 \pm 0.020)$ eV $= (172.8 \pm 1.9)$ kJ mol^{-1}.

In principle, the equation of the line in Fig. 8 completely describes the variation of ln τ with temperature, for a standard catholyte ($[S]_R = 4.5$ mol dm^{-3}, $[V^V]_R = 1.7$ mol dm^{-3}). Thus,

$$\ln\ \tau_R = B_R + \frac{m}{T} \qquad [21]$$

where τ_R and B_R correspond to the standard catholyte. For any solution with concentrations [S] and $[V^V]$

$$\ln\ \tau = \ln\ \tau_R + \beta_S([S] - [S]_R) + \beta_{V5}([V^V] - [V^V]_R) \qquad [22]$$

$$= B_R + \frac{m}{T} + \beta_S([S] - [S]_R) + \beta_{V5}([V^V] - [V^V]_R). \qquad [23]$$

Equation 23 summarizes the observed linear variation of induction time with $1/T$, [S] and $[V^V]$. It may be used to determine the induction time at any temperature T and concentrations [S] and $[V^V]$ based on the values of B_R and m (obtained from an Arrhenius plot such as Fig. 8 for a reference solution with concentrations $[S]_R$ and $[V^V]_R$) and the values of β_S and β_{V5} (obtained from plots such as Figs. 6 and 7).

Equation 23 may also be expressed in terms of the induction time τ_{std} for the reference catholyte at some standard temperature T_0. From Equation 21

$$\ln\ \tau_{std} = B_R + \frac{m}{T_0} \qquad [24]$$

Substituting Equation 24 in Equation 23,

$$\ln\ \tau = \ln\ \tau_{std} + m\left(\frac{1}{T} - \frac{1}{T_0}\right) + \beta_S\left([S] - [S]_R\right) + \beta_{V5}\left([V^V] - [V^V]_R\right) \qquad [25]$$

and

$$\tau = \tau_{std} \exp\left\{m\left(\frac{1}{T} - \frac{1}{T_0}\right) + \beta_S\left([S] - [S]_R\right) + \beta_{V5}\left([V^V] - [V^V]_R\right)\right\} \qquad [26]$$

Table III. Summary of parameters for a standard catholyte.

Standard Catholyte:		
Sulfate concentration	$[S]_R$	4.5 mol dm^{-3}
V^V concentration	$[V^V]_R$	1.7 mol dm^{-3}
Arrhenius Parameters:		
Intercept (Fig. 8)	B_R	−53.828
Slope (Fig. 8)	m	2.0785×10^4 K
Concentration coefficients of induction time:		
Sulfate concentration coefficient (Fig. 6)	β_S	2.073 mol^{-1} dm^3
V^V concentration coefficient (Fig. 7)	β_{V5}	−3.434 mol^{-1} dm^3
Induction time at standard temperature $T_0 = 298.15$ K	τ_{std}	7.9226×10^6 s

Values of the parameters in Equations 23–26 are summarized in Table III for a typical choice of reference catholyte.

Simulating catholyte stability.—Using Equations 23–26, we can simulate the value of induction time for precipitation at a temperature T for any electrolyte with concentrations of sulfate and V^V within the range of applicability of the equations. Typical results of such a simulation are shown in Fig. 9 where induction time is plotted against temperature for a series of catholytes, each with a total sulfate concentration of 4.5 mol dm^{-3}. As expected, the induction time decreases rapidly with temperature. The induction time also decreases with increasing concentration of V^V. Thus, for example, at 30°C a 1.6 mol dm^{-3} V^V solution is expected to be stable for ∼40 days while a 1.4 mol dm^{-3} V^V solution is expected to be stable for ∼82 days. Likewise, while a 1.6 mol dm^{-3} V^V solution is stable for ∼40 days at 30°C, it is stable for only ∼5 days at 40°C. Similar stability curves for several sulfate concentrations, each with a total V^V concentration of 1.5 mol dm^{-3}, are shown in Fig. 10. As in Fig. 9, the induction time decreases rapidly with increasing temperature. However, the induction time at any given temperature increases with increasing concentration of sulfate.

Such diagrams may be useful in predicting the stability of the catholyte in VFBs since they quantify the stability of V^V solutions of various compositions, as a function of temperature, using the induction time as a metric: the longer the induction time, the more stable the solution.

Other observations.—Some experiments were also carried out at lower concentrations of vanadium ($[V^V] < 1.4$ mol dm^{-3}). The results are compared in Fig. 11 with corresponding results at higher

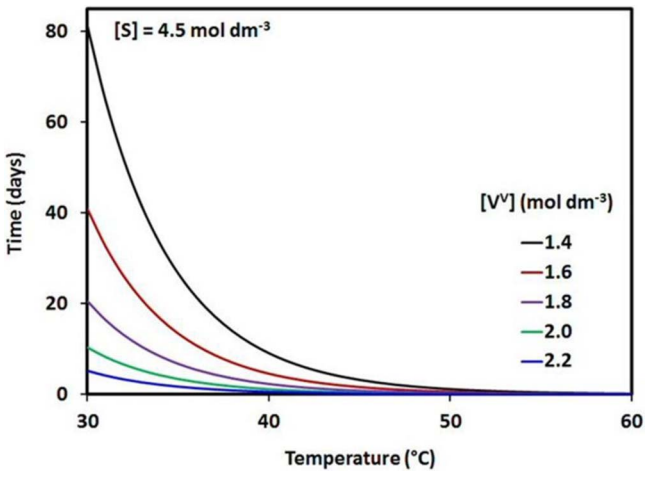

Figure 9. Simulated induction time for precipitation for a series of concentrations of V^V plotted against temperature. The sulfate concentration is 4.5 mol dm^{-3}.

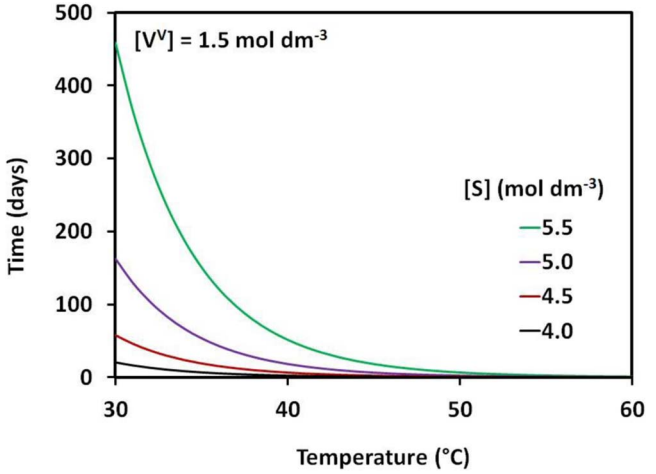

Figure 10. Simulated induction time for precipitation for a series of sulfate concentrations plotted against temperature. The of V^V concentration is 1.5 mol dm^{-3}.

concentrations. While the (log-linear) plot of induction time shows good linearity with $[V^V]$ at concentrations greater than 1.4 mol dm^{-3}, values of induction time at concentrations of 1 mol dm^{-3} and 1.2 mol dm^{-3} are above the extrapolated line. Only a limited number of experiments were carried out, but in general, these suggested that the Arrhenius slopes (activation energies) at lower concentration of V^V were somewhat higher. However, further work is necessary to more precisely quantify these effects.

Experiments on the effect of V^{IV} on the precipitation of V^V are made difficult by the formation[22,23,27] of a strongly absorbing mixed-valence complex, $V_2O_3^{3+}$, which darkens the solution at relatively low concentrations of V^{IV} and makes visual observation of the early stages of precipitation difficult. We carried out some experiments with relatively low concentrations of V^{IV} (∼10% of total vanadium) and these suggest that the induction time may be slightly increased by the presence of V^{IV}. However, the effect appeared to be quite small and further work is necessary to more precisely quantify it.

The mechanism of the processes leading to precipitation of V^V from catholytes[8,34,69,87–89] is not well understood. The pervanadyl ion

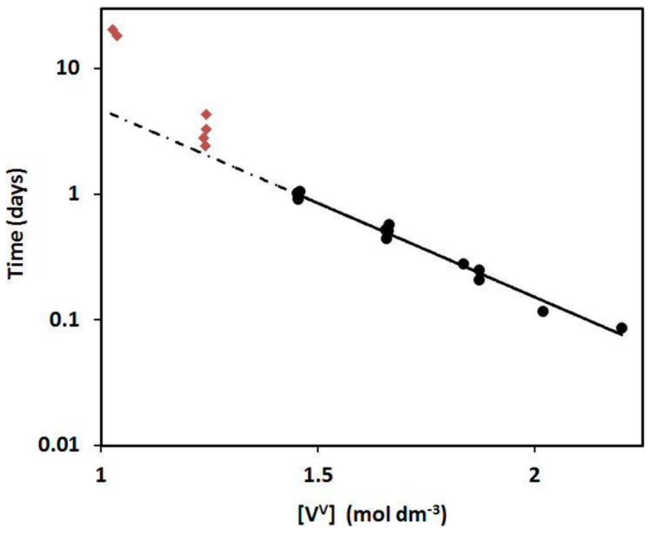

Figure 11. Induction time at 50°C for a sulfate concentration of 4.5 mol dm^{-3} plotted against vanadium concentration. The data for the black points ($[V^V] > 1.4$ mol dm^{-3}) is from Fig. 7 and the line represents the least-squares best fit to these points. Note that the red points (lower concentrations of V^V) fall above the trend line.

6. M. Skyllas-Kazacos, M. H. Chakrabarti, S. A. Hajimolana, F. S. Mjalli, and M. Saleem, *J. Electrochem. Soc.*, **158**, R55 (2011).
7. M. J. Watt-Smith, P. Ridley, R. G. A. Wills, A. A. Shah, and F. C. Walsh, *J. Chem. Technol. Biotechnol.*, **88**, 126 (2013).
8. S. Roe, C. Menictas, and M. Skyllas-Kazacos, *J. Electrochem. Soc.*, **163**, A5023 (2016).
9. A. Bourke, M. A. Miller, R. P. Lynch, X. Gao, J. Landon, J. S. Wainright, R. F. Savinell, and D. N. Buckley, *J. Electrochem. Soc.*, **163**, A5097 (2016).
10. A. Bourke, M. A. Miller, R. P. Lynch, J. S. Wainright, R. F. Savinell, and D. N. Buckley, *J. Electrochem. Soc.*, **162**, A1547 (2015).
11. M. A. Miller, A. Bourke, N. Quill, J. S. Wainright, R. P. Lynch, D. N. Buckley, and R. F. Savinell, *J. Electrochem. Soc.*, **163**, A2095 (2016).
12. A. Z. Weber and T. Van Nguyen, *J. Electrochem. Soc.*, **163**, Y1 (2016).
13. M. L. Perry and A. Z. Weber, *J. Electrochem. Soc.*, **163**, A5064 (2016).
14. D. Reed, E. Thomsen, B. Li, W. Wang, Z. Nie, B. Koeppel, J. Kizewski, and V. Sprenkle, *J. Electrochem. Soc.*, **163**, A5211 (2016).
15. H. H. Dewage, V. Yufit, and N. P. Brandon, *J. Electrochem. Soc.*, **163**, A5236 (2016).
16. R. M. Darling, A. Z. Weber, M. C. Tucker, and M. L. Perry, *J. Electrochem. Soc.*, **163**, A5014 (2016).
17. A. K. Manohar, K. M. Kim, E. Plichta, M. Hendrickson, S. Rawlings, and S. R. Narayanan, *J. Electrochem. Soc.*, **163**, A5118 (2016).
18. C. R. Dennison, E. Agar, B. Akuzum, and E. C. Kumbur, *J. Electrochem. Soc.*, **163**, A5163 (2016).
19. A. M. Pezeshki, R. L. Sacci, G. M. Veith, Thomas, A. Zawodzinski, and M. M. Mench, *J. Electrochem. Soc.*, **163**, A5202 (2016).
20. *Painesville Vanadium Redox Flow Battery Project, Technology Performance Report*, City of Painesville, Ashlawn Energy, LLC. (2015).
21. N. Tokuda, T. Kanno, T. Hara, T. Shigematsu, Y. Tsutsui, A. Ikeuchi, T. Itou, and T. Kumamoto, *SEI Tech. Rev.*, p. 88 (2000).
22. C. Petchsingh, N. Quill, J. T. Joyce, D. Ní Eidhin, D. Oboroceanu, C. Lenihan, X. Gao, R. P. Lynch, and D. N. Buckley, *J. Electrochem. Soc.*, **163**, A5068 (2016).
23. D. N. Buckley, X. Gao, R. P. Lynch, N. Quill, and M. J. Leahy, *J. Electrochem. Soc.*, **161**, A524 (2014).
24. M. Vynnycky, *Energy*, **36**, 2242 (2011).
25. G. Kear, A. A. Shah, and F. C. Walsh, *Int. J. Energy Res.*, **36**, 1105 (2012).
26. D. N. Buckley, X. Gao, R. P. Lynch, M. J. Leahy, A. Bourke, and G. Flynn, European Pat. EP 13195315 (2013).
27. X. Gao, R. P. Lynch, M. J. Leahy, and D. N. Buckley, *ECS Trans*, **45**, 25 (2013).
28. X. Gao, A. Bourke, R. P. Lynch, M. J. Leahy, and D. N. Buckley, *Conference Papers, The International Flow Battery Forum*, 20 (2013).
29. Z. Tang, D. S. Aaron, A. B. Papandrew, and T. A. Zawodzinski, *ECS Trans*, **41**, 1 (2012).
30. M. Skyllas-Kazacos and M. Kazacos, *J. Power Sources*, **196**, 8822 (2011).
31. N. Quill, R. P. Lynch, X. Gao, and D. N. Buckley, *The Electrochemical Society Meeting Abstract*, **MA2014-01**, 389 (2014).
32. A. H. Whitehead and M. Harrer, *J. Power Sources*, **230**, 271 (2013).
33. F. Rahman and M. Skyllas-Kazacos, *J. Power Sources*, **189**, 1212 (2009).
34. M. Vijayakumar, W. Wang, Z. Nie, V. Sprenkle, and J. Hu, *J. Power Sources*, **241**, 173 (2013).
35. H. Prifti, A. Parasuraman, S. Winardi, T. M. Lim, and M. Skyllas-Kazacos, *Membranes*, **2**, 275 (2012).
36. A. Bourke, R. P. Lynch, and D. N. Buckley, *ECS Trans*, **64**, 1 (2015).
37. A. Bourke, N. Quill, R. P. Lynch, and D. N. Buckley, *ECS Trans*, **61**, 15 (2014).
38. A. Bourke, N. Quill, R. P. Lynch, and D. N. Buckley, *Conference Papers, The International Flow Battery Forum*, 16 (2014).
39. A. Bourke, R. P. Lynch, and D. N. Buckley, *ECS Trans*, **53**, 59 (2013).
40. G. Oriji, Y. Katayama, and T. Miura, *J. Power Sources*, **139**, 321 (2005).
41. E. Sum and M. Skyllas-Kazacos, *J. Power Sources*, **15**, 179 (1985).
42. E. Sum, M. Rychcik, and M. Skyllas-Kazacos, *J. Power Sources*, **16**, 85 (1985).
43. D. Aaron, C. N. Sun, M. Bright, A. B. Papandrew, M. M. Mench, and T. A. Zawodzinski, *ECS Electrochem. Letters*, **2**, A29 (2013).
44. C. N. Sun, F. M. Delnick, D. S. Aaron, A. B. Papandrew, M. M. Mench, and T. A. Zawodzinski, *ECS Electrochem. Letters*, **2**, A43 (2013).
45. J. W. Lee, J. K. Hong, and E. Kjeang, *Electrochim. Acta*, **83**, 430 (2012).
46. M. Gattrell, J. Park, B. MacDougall, J. Apte, S. McCarthy, and C. W. Wu, *J. Electrochem. Soc.*, **151**, A123 (2004).
47. H. Kaneko, K. Nozaki, Y. Wada, T. Aoki, A. Negishi, and M. Kamimoto, *Electrochim. Acta*, **36**, 1191 (1991).
48. A. Di Blasi, O. Di Blasi, N. Briguglio, A. S. Aricò, D. Sebastián, M. J. Lázaro, G. Monforte, and V. Antonucci, *J. Power Sources*, **227**, 15 (2013).
49. W. Li, J. Liu, and C. Yan, *Carbon*, **55**, 313 (2013).
50. W. Zhang, J. Xi, Z. Li, H. Zhou, L. Liu, Z. Wu, and X. Qiu, *Electrochim. Acta*, **89**, 429 (2013).
51. J. Xi, W. Zhang, Z. Li, H. Zhou, L. Liu, Z. Wu, and X. Qiu, *Int. J. Electrochem. Sci.*, **8**, 4700 (2013).
52. Y. Men and T. Sun, *Int. J. Electrochem. Sci.*, **7**, 3482 (2012).
53. X. G. Li, K. L. Huang, S. Q. Liu, N. Tan, and L. Q. Chen, *Transactions of Nonferrous Metals Society of China (English Edition)*, **17**, 195 (2007).
54. M. A. Miller, R. F. Savinell, and J. S. Wainright, *The Electrochemical Society Meeting Abstract*, **MA2014-02**, 25 (2014).
55. L. Yue, W. Li, F. Sun, L. Zhao, and L. Xing, *Carbon*, **48**, 3079 (2010).
56. B. Sun and M. Skyllas-Kazacos, *Electrochim. Acta*, **37**, 2459 (1992).
57. E. Agar, C. R. Dennison, K. W. Knehr, and E. C. Kumbur, *J. Power Sources*, **225**, 89 (2013).
58. J. Friedl, C. Bauer, A. Rinaldi, and U. Stimming, *Carbon*, **63**, 228 (2013).
59. B. Sun and M. Skyllas-Kazacos, *Electrochim. Acta*, **37**, 1253 (1992).
60. Z. González, C. Botas, P. Álvarez, S. Roldán, C. Blanco, R. Santamaría, M. Granda, and R. Menéndez, *Carbon*, **50**, 828 (2012).
61. C. Flox, J. Rubio-García, M. Skoumal, T. Andreu, and J. R. Morante, *Carbon*, **60**, 280 (2013).
62. X. W. Wu, T. Yamamura, S. Ohta, Q. X. Zhang, F. C. Lv, C. M. Liu, K. Shirasaki, I. Satoh, T. Shikama, D. Lu, and S. Q. Liu, *J. Appl. Electrochem.*, **41**, 1183 (2011).
63. T. Yamamura, N. Watanabe, T. Yano, and Y. Shiokawa, *J. Electrochem. Soc.*, **152**, A830 (2005).
64. P. Chen, M. A. Fryling, and R. L. McCreery, *Analytical Chemistry*, **67**, 3115 (1995).
65. M. Gattrell, J. Qian, C. Stewart, P. Graham, and B. MacDougall, *Electrochim. Acta*, **51**, 395 (2005).
66. K. J. Kim, Y. J. Kim, J. H. Kim, and M. S. Park, *Materials Chemistry and Physics*, **131**, 547 (2011).
67. W. Li, J. Liu, and C. Yan, *Electrochim. Acta*, **79**, 102 (2012).
68. S. Zhong and M. Skyllas-Kazacos, *J. Power Sources*, **39**, 1 (1992).
69. J. Zhang, L. Li, Z. Nie, B. Chen, M. Vijayakumar, S. Kim, W. Wang, B. Schwnezer, J. Liu, and Z. Yang, *J. Appl. Electrochem.*, **41**, 1215 (2011).
70. M. Pourbaix, *Atlas of Electrochemical Equilibria in Aqueous Solutions*, National Association of Corrosion Engineers, 2nd ed (1974).
71. F. T. Silva and T. Ogasawara, *Transactions of the Institution of Mining and Metallurgy, Section C, Minerals Processing and Extractive Metallurgy*, **102**, C188 (1993).
72. M. Kazacos, M. Cheng, and M. Skyllas-Kazacos, *J. Appl. Electrochem.*, **20**, 463 (1990).
73. M. Skyllas-Kazacos, C. Menictas, and M. Kazacos, *J. Electrochem. Soc.*, **143**, L86 (1996).
74. D. Oboroceanu, N. Quill, C. Lenihan, D. Ní Eidhin, S. P. Albu, R. P. Lynch, and D. N. Buckley, *The Electrochemical Society Meeting Abstract*, **A02-0146**, New Orleans, USA (2017).
75. Y. Wen, Y. Xu, J. Cheng, G. Cao, and Y. Yang, *Electrochim. Acta*, **96**, 268 (2013).
76. M. Vijayakumar, L. Li, G. Graff, J. Liu, H. Zhang, Z. Yang, and J. Z. Hu, *J. Power Sources*, **196**, 3669 (2011).
77. M. Skyllas-Kazacos, M. Rychcik, R. G. Robins, A. G. Fane, and M. A. Green, *J. Electrochem. Soc.*, **133**, 1057 (1986).
78. M. Cheng, "Electrolyte Optimization and Studies for the Vanadium Redox Flow Battery", *MSc Thesis University of New South Wales* (1991).
79. D. Oboroceanu, N. Quill, C. Lenihan, D. Ní Eidhin, S. P. Albu, R. P. Lynch, and D. N. Buckley, *J. Electrochem. Soc.*, **163**(14), A2919 (2016).
80. P. Atkins and J. de Paula, *Physical Chemistry*, p.837, 10th ed., Oxford University Press (2014).
81. A. Ortega, *Int. J. Chem. Kinet.*, **33**, 343 (2001).
82. M. Pijolat and M. Soustelle, *Thermochim. Acta*, **525**, 93 (2011).
83. S. Ahmed, D. N. Buckley, S. Nakahara, T. T. Ahmed, and Y. Kuo, *J. Electrochem. Soc.*, **154**, D103 (2007).
84. E. J. Mittemeijer, *J. Mater. Sci.*, **27**, 3977 (1992).
85. F. Liu, F. Sommer, C. Bos, and E. J. Mittemeijer, *Int. Materials Reviews*, **52**, 193 (2007).
86. D. Oboroceanu, N. Quill, C. Lenihan, D. Ní Eidhin, S. P. Albu, R. P. Lynch, and D. N. Buckley, *ECS Trans*, **75**(18), 49 (2017).
87. M. Vijayakumar, Z. Nie, E. Walter, J. Hu, J. Liu, V. Sprenkle, and W. Wang, *ChemPlusChem*, **80**, 428 (2015).
88. X. Lu, *Electrochimica Acta*, **46**, 4281 (2001).
89. S. Peng, N. Wang, C. Gao, Y. Lei, X. Liang, S. Liu, and Y. Liu, *Int. J. Electrochem. Sci.*, **7**, 4388 (2012).
90. C. Madic, G. M. Begun, R. L. Hahn, J. P. Launay, and W. E. Thiessen, *Inorganic Chemistry*, **23**, 469 (1984).
91. J. Livage in, *Advanced Zeolite Science and Applications*, J. C. Jansen, M. Stocker, H. G. Karge, and J. Weitkamp, Editors, *Studies in Surface Science and Catalysis*, **85**, 1 (1994).
92. G. A. Pozarnsky and A. V. McCormick, *Chem. Mater.*, **6**, 380 (1994).